Nonlinear rovibrational polarization response of water vapor to ultrashort long-wave infrared pulses

K. Schuh, P. Rosenow, M. Kolesik, E. M. Wright, S. W. Koch, and J. V. Moloney

Phys. Rev. A **96**, 043818 — Published 9 October 2017

DOI: 10.1103/PhysRevA.96.043818

Nonlinear rovibrational polarization response of water vapor to ultrashort long-wave infrared pulses

K. Schuh,[1,*] P. Rosenow,[1] M. Kolesik,[1] E. M. Wright,[1] S. W. Koch,[1,2] and J. V. Moloney[1]

[1] *Arizona Center for Mathematical Sciences and College of Optical Sciences, University of Arizona, Tucson, Arizona 85721, USA*

[2] *Department of Physics and Materials Science Center, Philipps-University, 35032 Marburg, Germany*

We study the rovibrational polarization response of water vapor using a fully correlated optical Bloch equations approach employing data from the HITRAN database. For a 10 μm long-wave infrared pulse the resulting linear response is negative, with a negative nonlinear response at intermediate intensities and a positive value at higher intensities. For a model atmosphere comprised of the electronic response of Argon combined with the rovibrational response of water vapor this leads to a weakened positive nonlinear response at intermediate intensities. Propagation simulations using a simplified non-correlated approach show the resultant reduction in the peak filament intensity sustained during filamentation due to the presence of the water vapor.

PACS numbers: 42.50.Ct, 42.65.Sf, 42.68.Ay, 42.68.Ge

Filamentation allows for the transmission of laser pulses through the atmosphere with relatively stable peak intensities over long distances by balancing self-focusing (electronic Kerr) and defocusing (diffraction, plasma) contributions [1–3]. This phenomenon has possible applications in long-range free-space optical communication, remote sensing [4, 5], synthesis of ultrashort pulses by higher harmonics generation [6, 7] and lightning guiding [8–10], to name but a few. The atmospheric transparency windows in the mid-wave (MWIR, $3-5\,\mu$m) [11, 12] and long-wave infrared (LWIR, $8-12\,\mu$m) [13, 14] regimes are of particular interest. Studies of nonlinear responses in molecular gases have so far been limited to the response of the electrons (Kerr effect) and the increased polarizability of the electrons due to a rotational response of the nuclei (rotational Raman effect). While this approach is justified in the optical and near infrared spectral ranges, molecules can react strongly to MWIR and LWIR pulses in the form of rovibrational transitions. Most previous investigations have been limited to the linear response due to rovibrational transitions [13, 15], while studies of nonlinear rovibrational optical effects in molecular gases are scarce [16].

In this paper, we study the rovibrational polarization response of water vapor as representative of the nuclear response of the molecules present in air. Specifically, throughout we consider LWIR pulses with a carrier wavelength of $10\,\mu$m, which corresponds to 124 meV, and lies 50 meV above the rotational transitions and 50 meV below the rovibrational transitions of the lowest vibrational mode of water (this difference matches two thermal energies at room temperature). This corresponds to the transparency regime with minimal absorption but with potential for non-instantaneous polarization response. Moreover, the $8-12\,\mu$m wavelength range is dominated by the strong rotational transitions at lower energies, which produces a negative linear polarizability due to the nuclear response [15]. In turn the lower energy rotational transitions can also produce a negative nonlinear response for intermediate values of the intensity.

The remainder of this paper is organized as follows: In Sec. I we first present our model for the description of the rovibrational response of water vapor to LWIR pulses based a fully correlated optical Bloch equations approach employing data from the HITRAN database. The selection of relevant transitions and the evaluation of the linear and nonlinear responses is given in Secs. II-IV. Section V describes a model atmosphere composed of Argon and water vapor, and Sec. VI presents simulations of filamentation in the model atmosphere to elucidate the role of the rovibrational transitions.

I. MODEL

In order to model the polarization response of water vapor due to the nuclear motions we employ a fully correlated optical Bloch equations approach using data from the HITRAN database. We assume a set of rovibrational states labeled α, β and γ coupled by dipole transitions described by dipole matrix elements $d_{\alpha\beta}$. Here α, β, γ each contain a set of six quantum numbers, three for the rotational and vibrational modes each. For illustration Fig. 1(a) shows the energy spectrum of the rovibrational states versus the rotational quantum number, the energy being on the right hand vertical axis, and for various vibrational states indicated along the left hand vertical axis. Figure 1(b) illustrates some dipole allowed transitions, the key being that the rovibrational coupling leads to transfer of population and coherence between many levels, and can in no way be construed as a collection of two-level systems. Then in the presence of an external field E the Hamiltonian for the system is given by

$$H = \sum_{\alpha} \epsilon_{\alpha} a_{\alpha}^{\dagger} a_{\alpha} - \sum_{\alpha,\beta} d_{\alpha\beta} E a_{\alpha}^{\dagger} a_{\beta}, \qquad (1)$$

* kschuh@optics.arizona.edu

with energies ϵ_α, and creation and annihilation operators $a^\dagger_\alpha$ and a_α, respectively. This leads to the equations of motion

$$\mathrm{i}\hbar\frac{\partial}{\partial t}\langle a^\dagger_\alpha a_\beta\rangle = (\epsilon_\alpha - \epsilon_\beta)\langle a^\dagger_\alpha a_\beta\rangle + \sum_\gamma d^*_{\alpha\gamma}E\langle a^\dagger_\gamma a_\beta\rangle - d_{\beta\gamma}E\langle a^\dagger_\alpha a_\gamma\rangle, \quad (2)$$

for the expectation values of the occupations $f_\alpha = \langle a^\dagger_\alpha a_\alpha\rangle$ and microscopic polarizations $P_{\alpha\beta} = \langle a^\dagger_\alpha a_\beta\rangle$ (with $\alpha \neq \beta$). We account for line broadening by including an additional damping term $-i\hbar\Gamma P_{\alpha\beta}$ in the equation of motion for the polarization, with damping rate Γ, for which a constant value is used ($3\cdot 10^{-4}\,\mathrm{fs}^{-1}$) based on the almost constant values given in the database for the individual transitions.

We extract the dipole matrix elements, the energies and damping (line broadenings) of water from the HITRAN database [17]. While the energies can be extracted directly, the dipole matrix elements can be calculated from the absorption line intensities and occupations of the states involved which are assumed to be thermally populated at room temperature.

Here, the center wavelength $\lambda = 10\,\mu$m (124 meV) of the LWIR pulse lies between the rotational and first rovibrational transitions of the water molecule as illustrated in Fig. 2 which shows the linear absorption spectrum of water vapor according to the HITRAN database, the LWIR photon energy being indicated by the vertical arrow. We limit our calculation to the 12709 most important dipole transitions connecting 2574 rovibrational states. This corresponds to relatively few transitions compared to the total number of possible combinations of states, this being mainly due to forbidden transitions. However, from the 142045 transitions included in HITRAN we exclude most for numerical expediency and since they are rather weak or spectrally far detuned from the LWIR radiaiton. We checked that the neglected levels indeed have a negligible effect for the test case of a 50 fs pulse of peak intensity $7\cdot 10^{16}\,\mathrm{W/m^2}$.

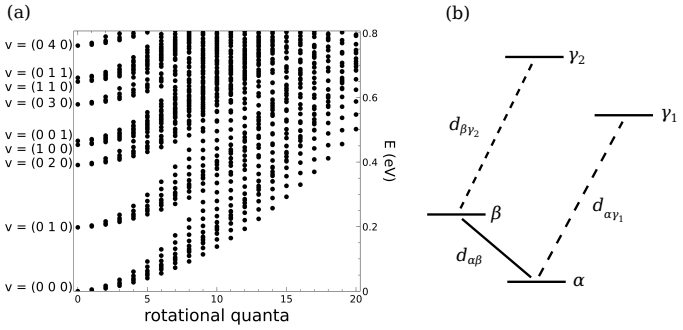

FIG. 1. (a) Energy spectrum of the rovibrational states, and (b) illustrates the coupling of dipole allowed transitions in (2). In (a) the energy is shown versus the (highest) rotational quantum number, the energy being on the right hand vertical axis, and for various vibrational states indicated along the left hand vertical axis. In (b), the solid line identifies a particular transition, for which the polarization is to be computed, and the dashed lines symbolize coupled transitions.

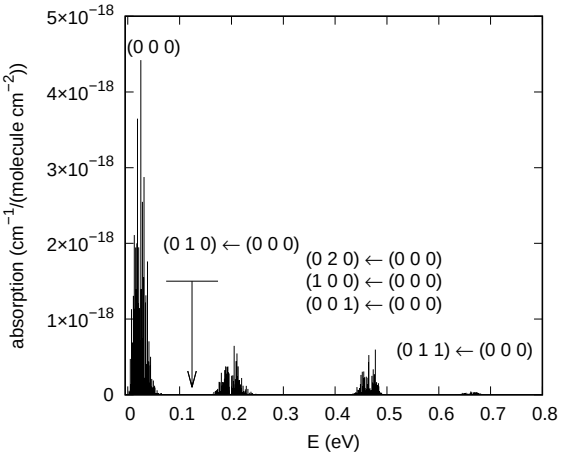

FIG. 2. Linear absorption spectrum of water vapor according to the HITRAN database, the LWIR photon energy being indicated by the vertical arrow, with the horizontal line showing the spectral width of a 50 fs pulse.

II. SELECTING THE TRANSITIONS

In the process of selecting transitions we first take only those with a lower state belonging to one of the 9 lowest vibrational states (up to energies of about 0.8 eV), there being little data regarding the higher energy vibrational states. In the next step, each selected transition is evaluated with respect to the wavelength of interest. In particular, for each transition a weighting factor

$$V_{\alpha\beta}(\omega) = \frac{|d_{\alpha\beta}|^2}{|\hbar\omega + \epsilon_\alpha - \epsilon_\beta|} \quad (3)$$

is calculated. All transitions with V above a set value will be taken into account. The appropriate value for the cut off was found by increasing its value until the result converged. In this work a value of $V_{\alpha\beta}(\omega) = 5\cdot 10^{11}\,\mathrm{pA^2\,fs^2\,nm^2/eV}$ was used.

This selection process eliminates weak and/or off-resonant transitions that contribute only marginally. The removal of transitions reduces the total absorption $\sum_{\alpha\beta} d^2_{\alpha\beta}$. Since we do not want to change the total absorption, we tested the effect of rescaling the transition dipole moments such that the total absorption is reproduced However, we find that this only has a negligible effect on the response, and shows that the most important transitions are captured by the weighting factor criterion.

III. LINEAR POLARIZATION RESPONSE

Based on previous calculations for water and 10 μm LWIR radiation [15], we know that the linear polarization response due to the rovibrational states is negative. This is the case since the lower rotational states are only about 50 meV lower in energy relative to the carrier frequency, leading to a negative polarizability. The vibrational transitions at higher energy which cause a positive polarization response cannot compensate this negative contribution. The electronic response, if included, is strong enough to compensate this negative response at this wavelength. However, in order to single out the rovibrational contribution to the polarization response, it is not included at this stage. For our calculations we assumed pure water vapor at atmospheric pressure.

Within our optical Bloch equation formalism the macroscopic polarization density $p(t)$ is calculated in terms of the microscopic polarizations $P_{\alpha\beta}(t)$ as

$$p(t) = 2N \sum_{\alpha\beta} \Re d_{\alpha\beta} P_{\alpha\beta}, \tag{4}$$

with N the particle density. According to linear response theory the macroscopic polarization can also be expressed generally as a functional of all past field strengths

$$p(t) = \int_{-\infty}^{t} E(t')\chi(t-t')\mathrm{d}t', \tag{5}$$

with $\chi(\tau)$ the memory function.

Figure 3 shows the linear polarization response of the rovibrational transitions of water for both (a) 200 fs, and (b) 50 fs duration 10 μm LWIR pulses. More specifically, in both cases the dashed green line shows the electric field $E(t)$ of the applied pulse and the solid black line shows $-p(t)$, the negative of the linear response, to aid in examination. For the 200 fs pulse in Fig. 3(a) we see that to a high degree $-p(t)$ tracks $E(t)$, implying an almost instantaneous response but with a negative polarizability, that is, $\chi(\tau) = C\delta(\tau)$ with C negative in Eq. (5). In contrast, for the 50 fs pulse in Fig. 3(b) non-instantaneous effects are more apparent, implying contributions to the memory function beyond the δ-function model. In particular, a clear phase shift between the field and polarization is present indicating energy transfer from the field to the nuclei in the first half of the pulse followed by the reverse in the second half. This effect is proportional to the time derivative of the pulse envelope and that is why it is much more pronounced for the shorter pulse. Also the different ratio between polarization and field amplitude for the two pulse durations in Fig. 3 is caused by the non-instantaneous nature of the linear response. Note, that the polarization component at the carrier frequency is not changed significantly by the pulse duration and that other frequency components cause the difference in amplitude.

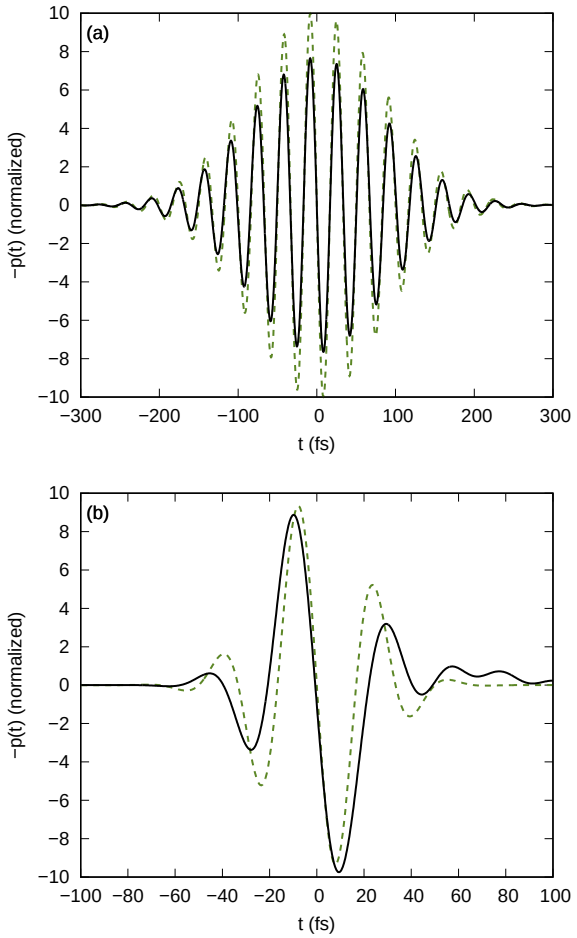

FIG. 3. (Color online) Linear polarization responses of the rovibrational transitions of water for (a) 200 fs and (b) 50 fs LWIR pulses: The dashed green line shows the shape of the applied electric field for each case.

IV. NONLINEAR POLARIZATION RESPONSE

Turning now to the nonlinear polarization response, Fig. 4 shows the negative polarization response $-p(t)$ of the rovibrational transitions of water to 200 fs LWIR pulses with peak intensities of 10^{16} (black line) and $10^{17}\,\mathrm{W/m^2}$ (blue line), the dashed green line showing the shape of the applied electric field. Close examination shows, that for the $10^{16}\,\mathrm{W/m^2}$ pulse both the linear and nonlinear responses are negative, whereas for the $10^{17}\,\mathrm{W/m^2}$ the nonlinear response is positive and can counter the linear response. The non-instantaneous nature of the nonlinear response is particularly evident for the higher pulse intensity (green line) as evidenced by the time-asymmetric polarization response in response to a time-symmetric pulse. In this case for shorter times the polarization is more negative compared to the linear response, while the negative linear response is partially compensated during the later parts of the pulse.

As a qualitative measure to explore the polarization re-

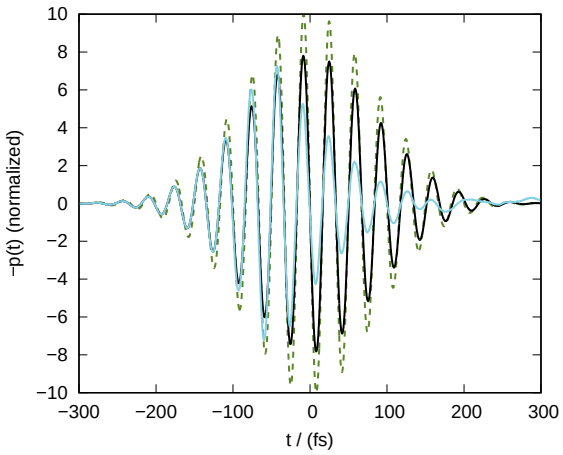

FIG. 4. (Color online) Polarization responses of the rovibrational transitions of water to 200 fs LWIR pulses with peak intensities of 10^{16} (black line) and 10^{17} W/m^2 (blue line) normalized to the electrical field. The dashed green line shows the shape of the applied electric field.

sponse, we use the susceptibility at the carrier frequency ω_c[18]

$$\chi_{\text{eff}}(\omega_c) = \frac{p(\omega_c)}{\epsilon_0 E(\omega_c)}, \tag{6}$$

which is shown in Fig. 5 for different pulse lengths as a function of peak intensity. While similar in their qualitative behavior, the nonlinearities vary significantly for each pulse length. With reference to Fig. 5(a) which shows the real part of the susceptibility, for lower intensities the nonlinear response is slightly positive, and partially counters the linear response. For intermediate values of the intensity (above about $5 \cdot 10^{15}$ W/m^2), the nonlinear response becomes negative as seen in Fig. 4(a) for the 10^{16} W/m^2 pulse (black line). Finally, for intensities above about $3 \cdot 10^{16}$ W/m^2 the trend towards positive nonlinear responses reverts with a sharp increase of the nonlinear polarization response. These trends are due to different transitions being dominant in different excitation regimes: As population is redistributed to higher states at high intensities this depletes the original states, that are thermally populated prior to the pulse, and this strengthens other transitions at different energies. Whilst this renders the rovibrational response very sensitive to the precise excitation conditions, the general trends alluded to above remain intact.

Figure 5(b) shows the corresponding variation of the imaginary part of the susceptibility with peak pulse intensity. Here we see that the absorption increases steadily with intensity as indicated by the increasingly negative imaginary part of the susceptibility. The increased linear absorption for shorter pulses is caused by the stronger spectral broadening (13 meV for 50 fs pulses) shifting the pulse spectrum into more strongly absorbing wavelengths. A saturation effect can be seen for the 200 fs

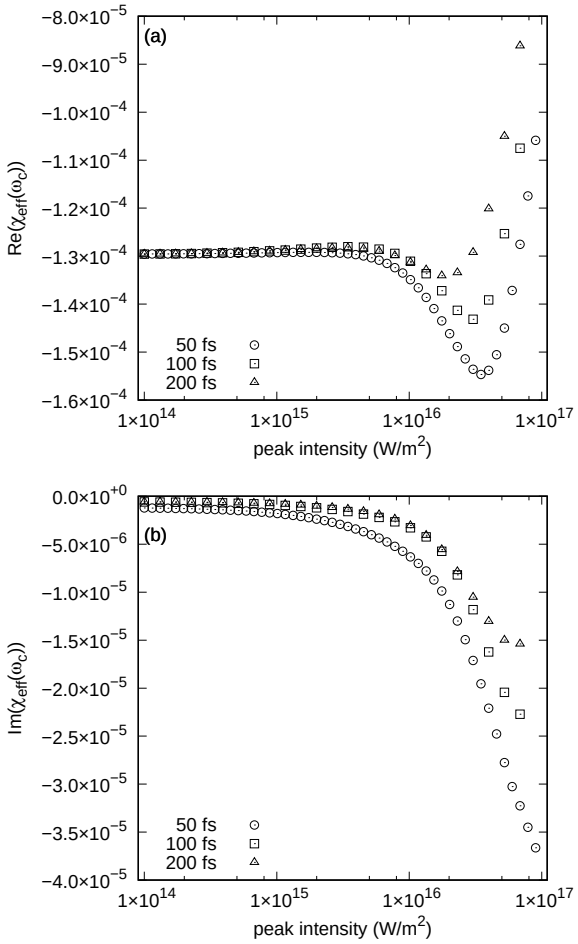

FIG. 5. (a) Real and (b) imaginary parts of the effective susceptibility $\chi_{\text{eff}}(\omega)$ at the carrier frequency as a function of peak intensity for 50 fs (circles), 100 fs (squares), and 200 fs (triangles) LWIR pulses.

pulse, indicating a depletion of low-energy states.

The broad changes in the occupations of the rovibrational states and the transitions are best exposed by examining the changes in absorption between the initial thermal distribution (blue line) and the excited system after a 50 fs LWIR pulse of peak intensity $7 \cdot 10^{16}$ W/m^2 (black line) as shown in Fig. 6. The first striking feature at high excitation is the strong expansion of the absorption bands thereby reducing the transparency windows drastically. Second the spectral regions marked by green horizontal lines exhibit gain following the excitation. This gain is due to population transfer into the upper levels of the respective transitions via other states, leading to population inversions between higher levels.

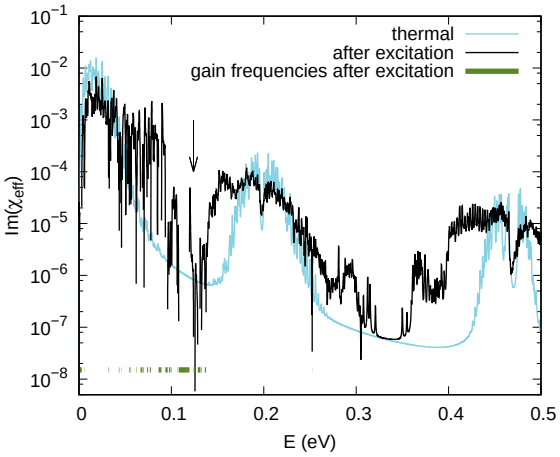

FIG. 6. (Color online) Absorption due to the rovibrational transitions for the initial thermal distribution (blue line) and after excitation with a 50 fs pulse of peak intensity $7 \cdot 10^{16}\,\mathrm{W/m^2}$ (black line). The vertical arrow indicates the carrier frequency of the LWIR pulse, and the spectral regions marked by thick green horizontal lines exhibit gain following the excitation

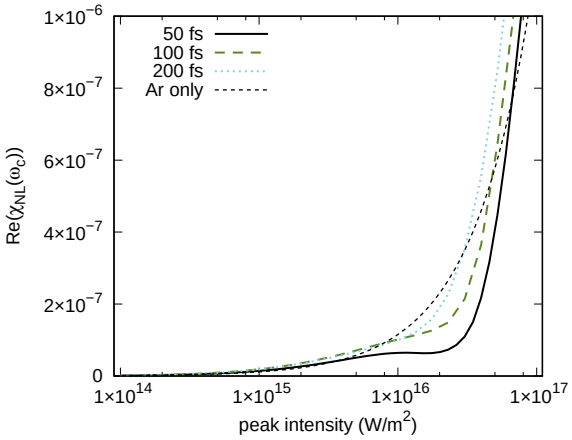

FIG. 7. (Color online) Real part of the effective nonlinear susceptibility at the carrier frequency as a function of peak intensity for 50 fs (solid black line), 100 fs (long-dashed green line), and 200 fs (dotted blue line) LWIR pulses in a model atmosphere composed of 99 % argon and 1 % water. The short-dashed black line indicates the effect of the electronic Kerr effect alone.

V. EFFECTIVE SUSCEPTIBILITY OF ARGON-WATER MIXTURE

As a model atmosphere, we use a gas at atmospheric pressure composed of 99 % argon and 1 % water. The water content corresponds to 32 % relative humidity at 25 °C. Filling the remaining part of the simulated gas with argon allows us to eliminate influences of the rovibrational transitions of other atmospheric molecules. We assume a Kerr coefficient $n_2 = 9.8 \cdot 10^{-24}\,\mathrm{m^2/W}$ due to electronic transitions for this gas based on the value for argon in Ref. [19]. The recently conducted first direct measurement of the Kerr coefficient for air at 10 μm yielded a value about five times this large [20]. However, given that the measured value of the Kerr coefficient for air includes contributions from rotational and Raman responses, here we used the cited value for Ar to capture the electronic response.

Figure 7 shows the real part of the effective nonlinear susceptibility at the carrier frequency as a function of peak intensity for 50 fs (solid black line), 100 fs (long-dashed green line), and 200 fs (dotted blue line) LWIR pulses in this model atmosphere, the electronic Kerr effect alone being indicated by the dashed black line. The addition of water vapor clearly leads to a significant departure from a Kerr-like behavior. In particular, instead of a susceptibility increasing linearly with intensity there is a more complex behavior including a significantly reduced gradient at intermediate intensities around $10^{16}\,\mathrm{W/m^2}$, indicating a reduced self focusing effect at these intensities.

The analysis of this section is based on assessing the nonlinear focusing effect at the carrier frequency, and is thus qualitative at best. In order to validate the basic picture in the next section we provide some illustrative filamentation simulations for LWIR pulses propagating in our model Ar-water atmosphere.

VI. SIMPLIFIED MODEL FOR PROPAGATION

It is currently not feasible to simulate Eqs. (2) in conjunction with the space-time resolved field propagation equation required to model filamentation. For this reason we here adopt the simplified equations of motion

$$\frac{\partial}{\partial t} f_\alpha = 2 \sum_\beta d_{\alpha\beta} E \Re \left(\frac{1}{\mathrm{i}\hbar} P_{\alpha\beta} \right), \tag{7}$$

$$\frac{\partial}{\partial t} P_{\alpha\beta} = -\Gamma P_{\alpha\beta} + \frac{1}{\mathrm{i}\hbar} \left[(\epsilon_\alpha - \epsilon_\beta) P_{\alpha\beta} + d_{\alpha\beta} E (f_\alpha - f_\beta) \right], \tag{8}$$

where we neglect couplings between different microscopic polarizations. This simplified model works reasonably well for intensities below $4 \cdot 10^{16}\,\mathrm{W/m^2}$ for the following reasons: By neglecting the direct coupling between polarizations sharing a common state, the impact of population transfers due to other transitions is not fully accounted for. This underestimates depletion effects and opens the possibility of negative populations at sufficiently high intensities. Moreover, dark polarizations can lead to mutual excitation and cause feedback to optically active polarizations, thereby influencing the macroscopic polarization response. The simplified model therefore applies for small depletion and this explains the limitation in peak intensity.

For the simulation of pulse propagation in the argon-water model atmosphere we use the unidirectional pulse

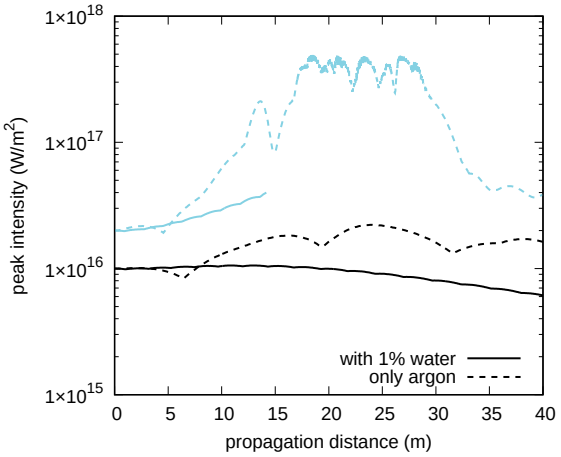

FIG. 8. (Color online) Maximum intensity over the transverse plane versus propagation distance for 100 fs LWIR pulses of peak powers 1.6 TW (black lines) and 3.2 TW (blue lines): The dash lines are for argon gas alone and the solid lines are with 1 % water vapor. In both cases the nuclear response of the water content reduces the self focusing leading to lower peak intensities compared to the case of pure argon cases.

propagation equation model (UPPE) [21] which allows for the inclusion of arbitrary nonlinear responses. In addition to the polarization response due to the rovibrational transitions for water vapor discussed above, we also include the electronic Kerr effect, with the Kerr coefficient $n_2 = 9.8{\cdot}10^{-24}\,\mathrm{m}^2/\mathrm{W}$ stated above[19], and multiphoton ionization appropriate to argon gas. The latter is implemented as a fit to the fully microscopic model as is described in detail in the supplemental information to [14].

Our goal with the simulations is to demonstrate the weakening of the pulsed self-focusing due to the electronic Kerr effect by the presence of the rovibrational polarization response. To this end Fig. 8 shows the maximum intensity over the transverse plane versus propagation distance for 100 fs LWIR pulses of peak powers 1.6 TW (black lines) and 3.2 TW (blue lines) with an initial waist radius of 1 cm: The dashed lines are for argon gas alone and the solid lines are with with 1 % water vapor. The case with 1.6 TW is slightly above the critical self-focusing power based on argon alone, and with no water vapor the peak intensity is seen to increase slightly with propagation (dashed black line). In contrast, the addition of water with its rovibrational response leads to a slightly decreasing intensity (solid black line) due to the negative nonlinearities discussed above. For the 3.2 TW peak power (blue lines) with about two critical powers the situation is similar, but here the self focusing is not turned into defocusing but rather the focusing is significantly weakened. The results for the cases with water vapor are limited in propagation distance by the intensity limitations of the simplified approximation employed, but the trends are clear.

VII. SUMMARY AND CONCLUSIONS

In summary, we have presented a fully correlated optical Bloch equation approach employing the HITRAN database to evaluate the nonlinear rovibrational response of water vapor to LWIR pulses, concentrating here on a 10 μm center wavelength. The linear response is found to be negative due to active rotational transitions below the carrier frequency, and to exhibit a non-instantaneous response. For intermediate intensities the nonlinear contribution to the response is negative, but becomes positive at higher intensities. For an argon-water model atmosphere, the rovibrational response of the water is found to weaken the electronic Kerr effect at intermediate intensities. These basic findings were validated in simulations of filamentation in the argon-water model atmosphere using a simplified model valid at low intensities, and for which the peak intensity of the propagating filament is reduced by the presence of the rovibrational transitions.

Our goal with this paper is to initiate the theoretical study and simulation of the rovibrational polarization response of molecules. The rovibrational response will be particularly important for pulse propagation in air in the long-wave infrared regime that is currently of great interest, and we hope our work stimulates experiments to validate and extend our work. Much work needs to be done to extend our model and simulations, and we mention a few areas. First, the data extracted from the HITRAN database is not complete. In particular, transitions between states with low occupations in a thermal state of the system are missing from the database, since they do not contribute to the linear properties of the system significantly. However, such transitions can contribute to the nonlinear response at high intensities. It is not abundantly clear at which intensity this becomes important. Furthermore, our model does not include effects on the rovibrational transitions due to changes of the electronic wave function and vice versa.

ACKNOWLEDGMENTS

This material is based upon work supported by the Air Force Office of Scientific Research under Grant No. FA9550-16-1-0088.

[1] A. Braun, G. Korn, X. Liu, D. Du, J. Squier, and G. Mourou, Opt. Lett. **20**, 73 (1995).
[2] P. Panagiotopoulos, P. Whalen, M. Kolesik, and J. V. Moloney, Nature Photonics **9**, 543 (2015).
[3] A. V. Mitrofanov, A. A. Voronin, D. A. Sidorov-Biryukov, A. Pugžlys, E. A. Stepanov, G. Andriukaitis,

T. Flöry, S. Ališauskas, a. B. Fedotov, A. Baltuška, and a. M. Zheltikov, Sci. Rep. **5**, 8368 (2015), arXiv:1410.2647v1.
[4] P. Rairoux, H. Schillinger, S. Niedermeier, M. Rodriguez, F. Ronneberger, R. Sauerbrey, B. Stein, D. Waite, C. Wedekind, H. Wille, L. Wöste, and C. Ziener, Appl. Phys. B **71**, 573 (2000).
[5] I. Dicaire, V. Jukna, C. Praz, C. Milián, L. Summerer, and A. Couairon, Laser Photonics Rev. **10**, 481 (2016).
[6] W. Chu, G. Li, H. Xie, J. Ni, J. Yao, B. Zeng, H. Zhang, C. Jing, H. Xu, Y. Cheng, and Z. Xu, Laser Phys. Lett. **11**, 015301 (2014).
[7] A. Couairon, A. Lotti, D. Faccio, P. Di Trapani, D. S. Steingrube, E. Schulz, T. Binhammer, U. Morgner, M. Kovacev, and M. B. Gaarde, Pramana - J. Phys. **83**, 221 (2014).
[8] R. P. Fischer, A. C. Ting, D. F. Gordon, R. F. Fernsler, G. P. DiComo, and P. Sprangle, IEEE Trans. Plasma Sci. **35**, 1430 (2007).
[9] A. Houard, C. D'Amico, Y. Liu, Y. B. Andre, M. Franco, B. Prade, A. Mysyrowicz, E. Salmon, P. Pierlot, and L. M. Cleon, Appl. Phys. Lett. **90**, 171501 (2007).
[10] F. Théberge, J.-F. Daigle, J.-C. Kieffer, F. Vidal, and M. Châteauneuf, Sci. Rep. **7**, 40063 (2017).
[11] H. Liang, D. L. Weerawarne, P. Krogen, R. I. Grynko, L. Chien-Jen, B. Shim, Kärtner, and K.-H. Hong, Optica **3**, 678 (2016).
[12] A. Zheltikov, J. Phys. B: At. Mol. Phys. **50**, 092001 (2017).
[13] P. Panagiotopoulos, K. Schuh, M. Kolesik, and J. V. Moloney, J. Opt. Soc. Am. B **33**, 2154 (2016).
[14] K. Schuh, M. Kolesik, E. M. Wright, J. V. Moloney, and S. W. Koch, Phys. Rev. Lett. **118**, 063901 (2017).
[15] R. J. Mathar, Appl. Opt. **43**, 928 (2004).
[16] J. K. Wahlstrand, S. Zahedpour, Y. H. Cheng, J. P. Palastro, and H. M. Milchberg, Phys. Rev. A **92**, 063828 (2015), arXiv:1510.04553.
[17] L. S. Rothman, I. E. Gordon, A. Barbe, D. C. Benner, P. F. Bernath, M. Birk, V. Boudon, L. R. Brown, A. Campargue, J.-P. Champion, *et al.*, J. Quant. Spect. Rad. Trans. **110**, 533 (2009).
[18] P. Béjot, E. Cormier, E. Hertz, B. Lavorel, J. Kasparian, J. P. Wolf, and O. Faucher, Phys. Rev. Lett. **110**, 043902 (2013), arXiv:1206.4906.
[19] S. Zahedpour, J. K. Wahlstrand, and H. M. Milchberg, Opt. Lett. **40**, 5794 (2015).
[20] J. J. Pigeon, S. Y. Tochitsky, E. C. Welch, and C. Joshi, Opt. Lett. **41**, 3924 (2016).
[21] M. Kolesik and J. V. Moloney, Phys. Rev. E **70**, 036604 (2004).